J Mater Sci (2023) 58:4637–4656

Metals & corrosion

Investigation on gradual degradation of mechanical property and microstructure in 9% Cr heat-resistant steels via interrupted creep test

Genqi Tian[1,2,3], Bo Mao[1], Yuantao Xu[1], Liming Fu[1,2,*], Zuogui Zhang[3], Yanfeng Wang[3], and Aidang Shan[1,2,*]

[1] School of Materials Science and Engineering, Shanghai Jiao Tong University, Shanghai 200240, People's Republic of China
[2] Shanghai Key Laboratory of High Temperature Materials and Precision Forming, Shanghai Jiao Tong University, Shanghai 200240, People's Republic of China
[3] Shanghai Power Equipment Research Institute Co., Ltd, Shanghai 200240, People's Republic of China

Received: 9 October 2022
Accepted: 9 February 2023
Published online: 23 February 2023

ABSTRACT

High-temperature strength and microstructure stability in heat-resistant steels are the major concerns for their practical applications. A comprehensive understanding of the microstructure evolution and mechanical property degradation during creep exposure is of significant importance for safety operations. In this work, a series of interrupted creep tests of 9% Cr steels were conducted at 873 K and 160 MPa exposed to different creep durations. The gradual degradation of mechanical properties and microstructure evolution such as dislocation density, martensite lath, precipitates and grain boundary characteristics were studied. It was found that the high-temperature yield strength and micro-hardness significantly decreased from the initial state to 1000 h duration then kept relatively stable to 1500 h duration, and gradually declined until rupture. The degradation of mechanical properties in primary creep stage was mainly attributed to decline in dislocation density and coarsening of martensite lath. Coarsening of martensite lath, as well as precipitation strengthening played a significant role in secondary creep stage. In tertiary creep stage, synergistic effect of coarsening of martensite lath and precipitates and decline of dislocation density resulted in accelerated degradation of mechanical properties. The precipitation of Laves phase in early stage provided additional strengthening effect and compensated for the strength loss caused by the coarsening of martensite lath, contributing to the stability of mechanical properties from 1000 to 1500 h. Moreover, the growth of Laves phase induced insignificant stain concentration and ductility deterioration. Quantitative

Handling Editor: Megumi Kawasaki.

Address correspondence to E-mail: lmfu@sjtu.edu.cn; adshan@sjtu.edu.cn

https://doi.org/10.1007/s10853-023-08296-8

relationships between microstructure and mechanical properties were established and well-validated by experimental results.

Introduction

The rapid development of ultra-supercritical (USC) power plants in the past decades have raised a critical need for the metallic components with excellent high-temperature engineering performance to ensure their thermal efficiency and reliability [1]. Ferritic–martensitic 9% Cr heat-resistant steels (9% Cr steels) have been widely utilized as key components in USC power plants and identified as promising candidates of structural material in Generation IV nuclear reactors [2, 3], due to their excellent mechanical properties, high thermal conductivity, low thermal expansion coefficient, good weldability and high inherent void swelling resistance to neutron irradiation [3–5]. The sufficient mechanical properties and stability of 9% Cr steels are crucial to the safe and efficient operation of USC power plant in design life.

The 9% Cr steels are mainly subjected to long-term exposure of high-temperature and steam pressure service environment, and therefore creep rupture is the main mechanism responsible for their failure in USC power plants [6]. Several microstructure evolution mechanisms associated with creep failure have been proposed, such as the declination of dislocation density [7, 8], widening of martensite lath [9, 10], precipitation and coarsening of Laves phase [11, 12] and modified Z-phase [13, 14], and Type IV failure in welded joint [15]. As the creep process proceeds, micro-hardness [16–18] and strength [19, 20] of the steels will inevitably deteriorate during the high-temperature exposure, which pose a serious threat on the safe operation of USC power plants and electricity supply. In engineering practice, the residual micro-hardness [16, 17] and strength are regarded as key indicators in regular metal supervision of components and estimation of remaining life.

Due to its scientific and practical significance, extensive efforts have been paid to investigate the evolution of microstructure and mechanical property of 9% Cr steels subjected to high-temperature exposure. For instance, Guo et al. [21] studied the degradation of strength, micro-hardness and microstructure of P92 after aging at 923 K from 200 to 11,000 h. It was found that the strength increased slightly in initial stage then continued to decrease after 500 h, whereas the micro-hardness exhibited a continuous declination. They provided systematic investigation on mechanical degradation during long-term aging, while stress-free state cannot reflect actual microstructure evolution under service condition. Some researchers compared the microstructure characteristics of the final creep-ruptured specimens with as-received condition. For instance, Panait [22, 23] found a significant decrease in hardness after creep for 113,431 h at 873 K in P91 steel, along with significant recovery of the matrix and coarsening of $M_{23}C_6$ carbides and Laves phase. Nie et al. [24] observed recovery of martensite lath and coarsening of precipitates during creep in T92 steel, and they also reported creep cavities nucleated at the interface of large Laves phase particles, thus aggravated the creep-rupture process.

These research results provided insightful knowledge on the microstructure and property evolution of 9% Cr steels from different viewpoints. However, few studies have been conducted to investigate the progressive degradation of mechanical property and microstructure in the intermediate stages via interrupted creep test [25–28], which are crucial for safety evaluation. Meanwhile, systematic investigations of the relationship between the microstructure evolution and mechanical property degradation were scarcely reported. In particular, the role of Laves phase on the mechanical property of 9% Cr steels during creep remains controversial. Ennis [29] suggested that precipitation of Laves phase depletes Mo and W in matrix and thus reduces solution strengthening. Coarsened Laves phase particles on boundaries tend to trigger creep cavities and brittle fracture [18]. However, other researchers [4, 21] demonstrated that Lave phase mainly contribute to precipitation strengthening before aggregation. Therefore, it is imperative to perform interrupted creep tests to thoroughly investigate the progressive property degradation and microstructure and clarify damage mechanisms of microstructure from initial state to rupture.

To systematically investigate the progressive degradation of mechanical property and

microstructure of 9% Cr steels, a series of interrupted creep test were conducted in this study. Then micro-hardness measurement and high-temperature tensile tests were performed on the interrupted creep specimens. Meanwhile, the microstructure evolution such as martensite lath, dislocation density and precipitates was also analyzed in detail. The aim of this research is to clarify damage mechanisms of microstructure at specific stage and establish quantitative relationships between residual mechanical properties and microstructure features. Moreover, the role of Laves phase in mechanical property of 9% Cr steels during creep will be also discussed. These experiment results of interrupted creep specimens provide valuable guidance for the estimation of creep damage and residual life in engineering application.

Materials and experiment

Materials

9% Cr heat-resistant steel pipe with an outer diameter of 457 mm and a wall thickness of 90 mm was used in this study. The hot-extruded pipes were normalized at 1323 K for 4 h, and tempered at 1033 K for 6 h. All the specimens were cut from the outer section of the pipe along tangential direction. Chemical composition of this steel is listed in Table 1.

Mechanical property tests

In order to investigate the effect of creep damage on subsequent tensile behavior, experiments were conducted in three steps. Firstly, a series of regular creep tests were conducted at 873 K till fracture to get creep curves under different stress (160 MPa, 180 MPa, 190 MPa, 200 MPa, 210 MPa, 220 MPa). Then, a series of interrupted creep tests were conducted at 873 K and 160 MPa to reach predetermined lifetime at regular intervals (500 h, 1000 h, 1500 h, 2000 h, 2500 h and fractured specimen at 2975 h). Afterward, all the interrupted creep specimens were machined into tensile specimens to evaluate their high-temperature tensile properties. The tensile tests were performed at 873 K and a constant strain rate of $0.00025\ s^{-1}$. Furthermore, microhardness of the as-received and crept specimens of 9% Cr steel were measured using Vickers Hardness Tester (Omnitech-S) with a load of 0.1 kg and dwell time of 10 s. The average values and standard deviation of 15 measurements were taken to describe the micro-hardness at each state. A slice cut from grip section represents aging state was also analyzed. The schematic illustration and the geometry parameters of the specimens subjected to regular creep tests, interrupted creep tests, aging tests and tensile tests are shown in Fig. 1.

Microstructure characterization

After interrupted creep tests, the materials were also longitudinally sectioned and prepared for microstructure characterization, as shown in Fig. 1d. Metallographic structure investigations were carried out by using a Zeiss AXIOVERT 200MAT optical microscope (OM). The strain distribution analyzed by transmission Kikuchi diffraction (TKD) technique and crystallographic features were evaluated using a MIRA3 scanning electron microscope (SEM) equipped with energy-dispersive X-ray spectrometer (EDS) and electron back-scattered diffraction (EBSD) detectors. Samples for EBSD characterization were ion beam polished via Gatan 697 Ilion II polishing system, and the data were analyzed via HKL Channel 5 software developed by Oxford Instruments. The nanoscale microstructure features, such as martensite lath and precipitate morphologies, were investigated with a JEOL JEM-2100 transmission electron microscope (TEM) equipped with an Oxford EDS detector. Thin foils for TKD and TEM observations were prepared by electropolishing in a Struers (Tenupol-5) machine at 20° C, and the electrolyte consisted of 7% perchloric acid and 93% alcohol. The average martensite lath width and standard deviation were calculated by linear intercept method in transverse direction from 20 TEM micrographs, about 150 laths per specimen. The precipitate phases were identified by EDS and selected area electron diffraction (SAED), and their sizes were measured from TEM micrographs via Image-Pro Plus software. The area fraction

Table 1 Chemical composition of the as-received 9% Cr steels (wt%)

Composition	C	Mn	Si	Cr	Mo	W	V	N	Ni	Al	Nb	Fe
Content	0.11	0.46	0.15	8.56	0.43	1.74	0.17	0.048	0.23	0.007	0.076	Bal

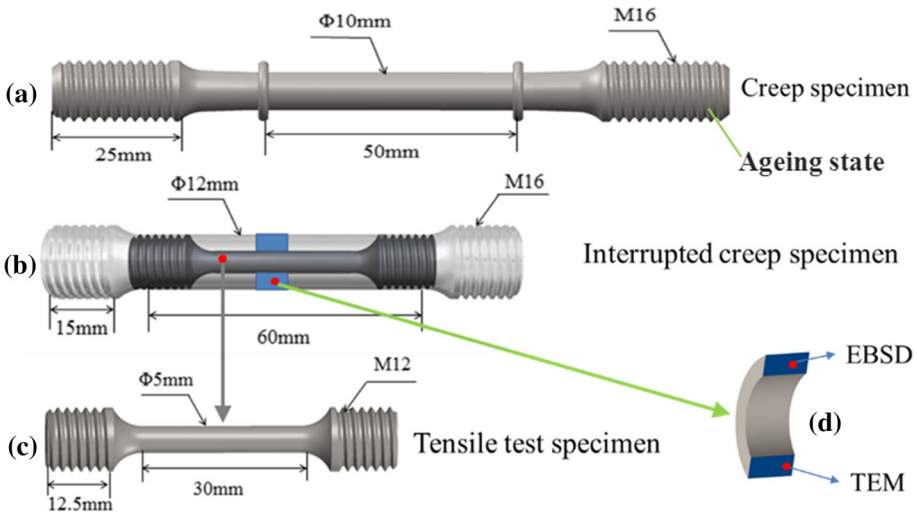

Figure 1 Schematic illustration and the geometry parameters of the specimens subjected to **a** regular creep tests, **b** interrupted creep tests, **c** tensile tests and **d** microstructure characterization.

and the mean size of the precipitates were measured by taking about 15 TEM micrographs, corresponding to 400 ~ 600 particles per specimen. X-ray diffractometer (Rigaku D/max-2500, CuKα, λ = 1.5418 Å) was used to measure the dislocation density in the specimen at a working voltage of ~ 40 kV, a current of ~ 40 mA, scanning speed of ~ 0.5° min^{-1} and an angular interval of ~ $20° \leq 2\theta \leq 145°$. Calculation method of the dislocation density from XRD results can be referred to method in literature [30–32].

Results

Microstructure and creep deformation behavior of as-received material

The initial microstructure of the 9% Cr steels prior to creep tests is depicted in Fig. 2. It was observed that the material exhibited a typical tempered martensite microstructure as shown in the OM image in Fig. 2a. The prior austenite grain boundaries (PAGBs) were marked by the yellow dash line, and the grain size was estimated to be around 40 μm. Some typical precipitates such as MX carbonitrides and $M_{23}C_6$ carbides can be detected and marked as A, B and C in TEM micrograph in Fig. 2b. By identifying the phase composition (Fig. 2c, d and e) and structure through EDS and SAED, it can be seen that MX precipitates mainly existed in the intra-lath region, whereas most of $M_{23}C_6$ carbides located at lath boundaries and a few of them occurred in the intra-lath region, as shown in Fig. 2b. In addition, detailed observation indicated that no Laves phase was observed in as-received specimen.

Creep curves at various stresses ranging from 160 to 220 MPa are depicted in Fig. 3a. The creep deformation of 9% Cr steels can be divided into primary creep stage, secondary creep stage and tertiary creep stage. The minimum creep rates can be described by modified version of Mukherjee-Bird-Dorn [33] creep equation as $\dot{\varepsilon}_{\min} = A\left(\frac{\sigma-\sigma_{th}}{E}\right)^n \exp\left(-\frac{Q_c}{RT}\right)$, where A is a constant, n is the stress exponent, Q_c is the creep activation energy, σ is applied stress,σ_{th} is threshold stress, E is the elastic modulus, R is the universal gas constant, and T is the temperature in Kelvin.

The variation of minimum creep rates $\dot{\varepsilon}_{\min}$ with the normalised creep stress by elastic modulus $((\sigma - \sigma_{th})/E)$ on bilogarithmic scale is depicted in Fig. 3b. The obtained stress exponent $n \approx 5$ indicated the rate-controlling creep mechanism was dislocation climb [33, 34]. According to the creep curve at 160 MPa and the interrupted time (500 h, 1000 h, 1500 h, 2000 h, 2500 h, and rupture time 2975 h) listed in sub-Sect. "Mechanical property tests," it can be determined that the corresponding creep strain at the interrupted time was 1.6%, 2.3%, 2.8%, 3.5%, 4.5%, and 19% (fracture creep strain), respectively, which cover the whole creep stages. The microstructure observation of these interrupted specimens is described in the following subsections.

Microstructure evolution of interrupted creep specimens

The 9% Cr steels exhibit a typical hierarchical microstructure, which consists of prior austenite grains, packets, blocks, and martensite

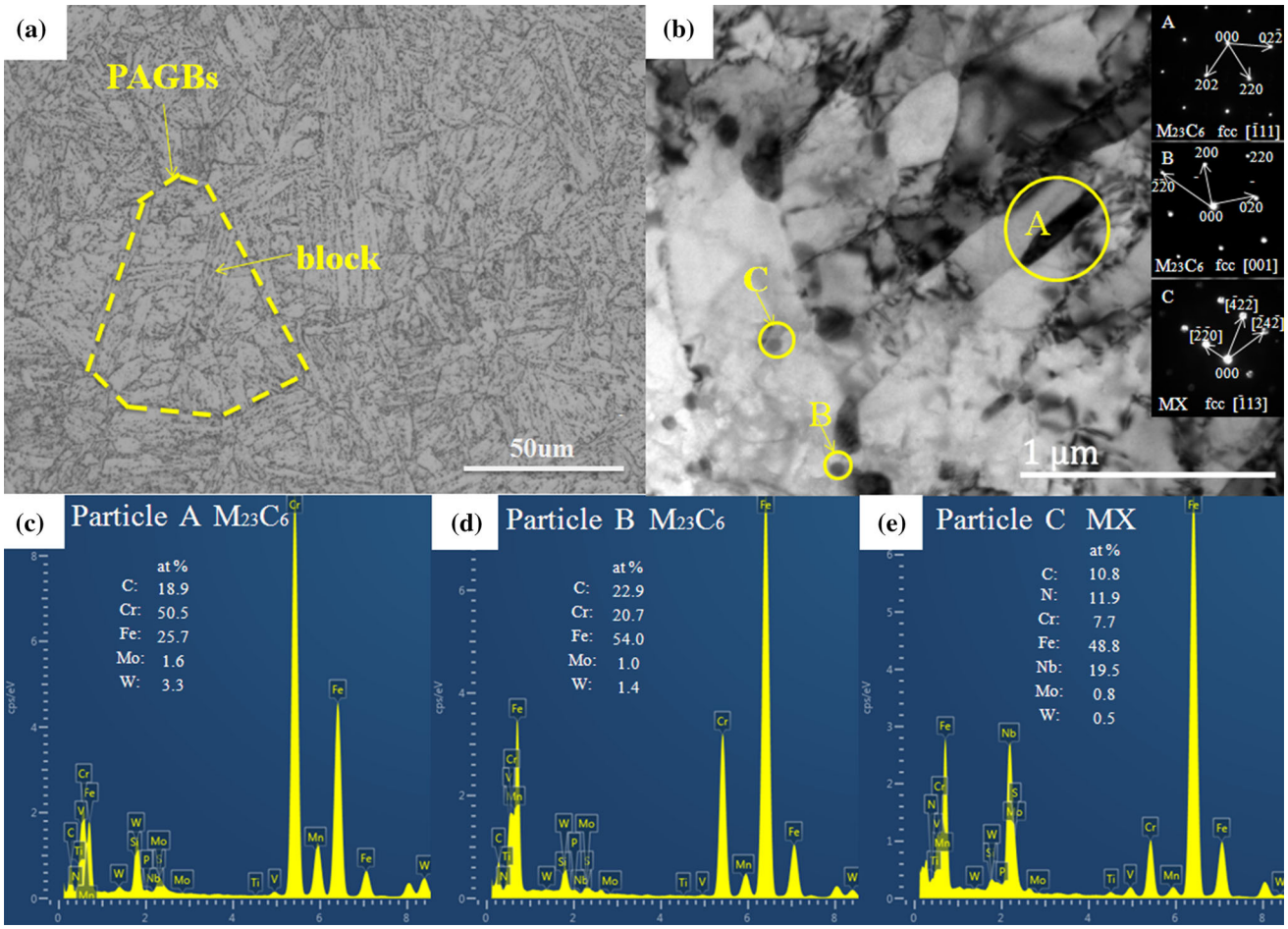

Figure 2 Microstructures of as-received materials: **a** Optical micrograph, **b** TEM micrograph, **c–e** EDS of $M_{23}C_6$ and MX precipitates.

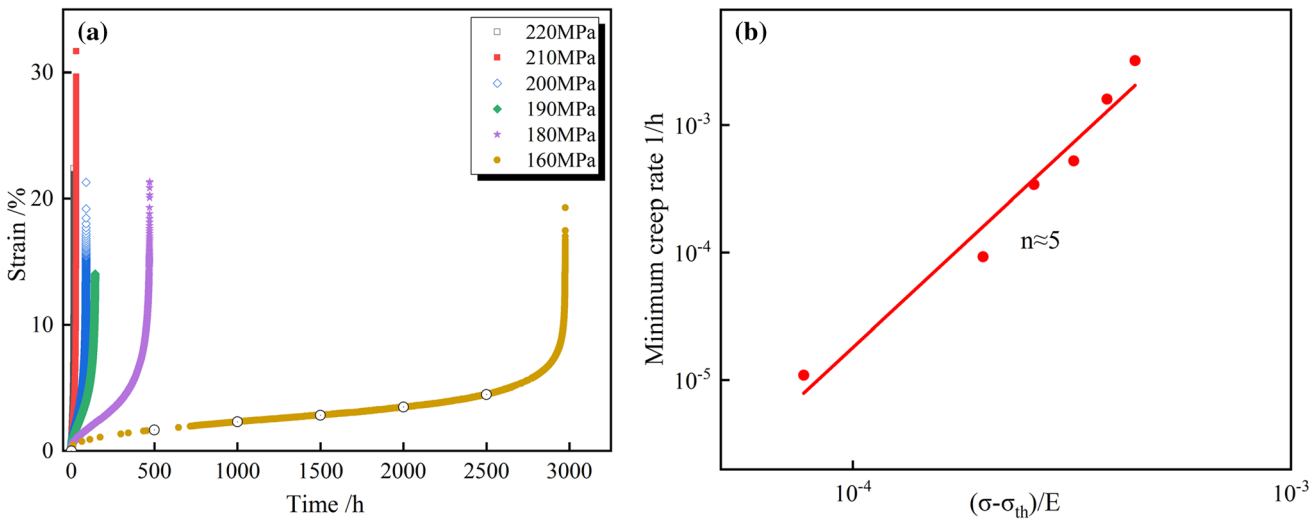

Figure 3 Creep behavior of as-received materials at 873 K: **a** creep curves at different stress and **b** variation of minimum creep rate with normalized creep stress.

laths/subgrains. The excellent high-temperature strength stems from high dislocation density, fine martensite lath, together with solid-solution strengthening by Mo and W atoms and precipitation strengthening by MX precipitates and $M_{23}C_6$ carbides [35, 36]. These microstructure features will evolve inevitably during creep service.

Recovery of martensite lath

The martensite lath structure is also called subgrain structure because of the low-angle grain boundaries between adjacent laths, and the laths tend to evolve into rounded eventually. Microstructure of the subgrains of crept samples and the evolution of martensite lath width is shown in Fig. 4a–c and e. It can be seen that the martensite lath width gradually increased with increasing creep time from initial state to 2000 h, and kept relatively stable until rupture. Similar observation was also reported by Xiao et al. [37], in which the microstructure evolution of G115 steel at 923 K and 140 MPa was investigated.

Evolution of dislocation substructure

It is well known that an extremely high density of dislocations was introduced into tempered martensite ferritic steels during the martensite transformation [7]. Unfortunately, there were sparse quantitative dislocation density data available in literature during the creep duration. TEM, XRD, and EBSD methods were usually employed to measure dislocation density [8, 30, 31, 38]. The XRD method was usually the most preferred due to its ability to obtain macroscopic and comprehensive dislocation density data. The evolution of dislocation density at different creep duration is indicated in Fig. 5b, and corresponding modified Williamson-Hall plots are shown in Fig. 5a, where $K = 2\sin\theta/\lambda$ and $\Delta K = 2\cos\theta\Delta\theta/\lambda$, θ and $\Delta\theta$ represent the diffraction

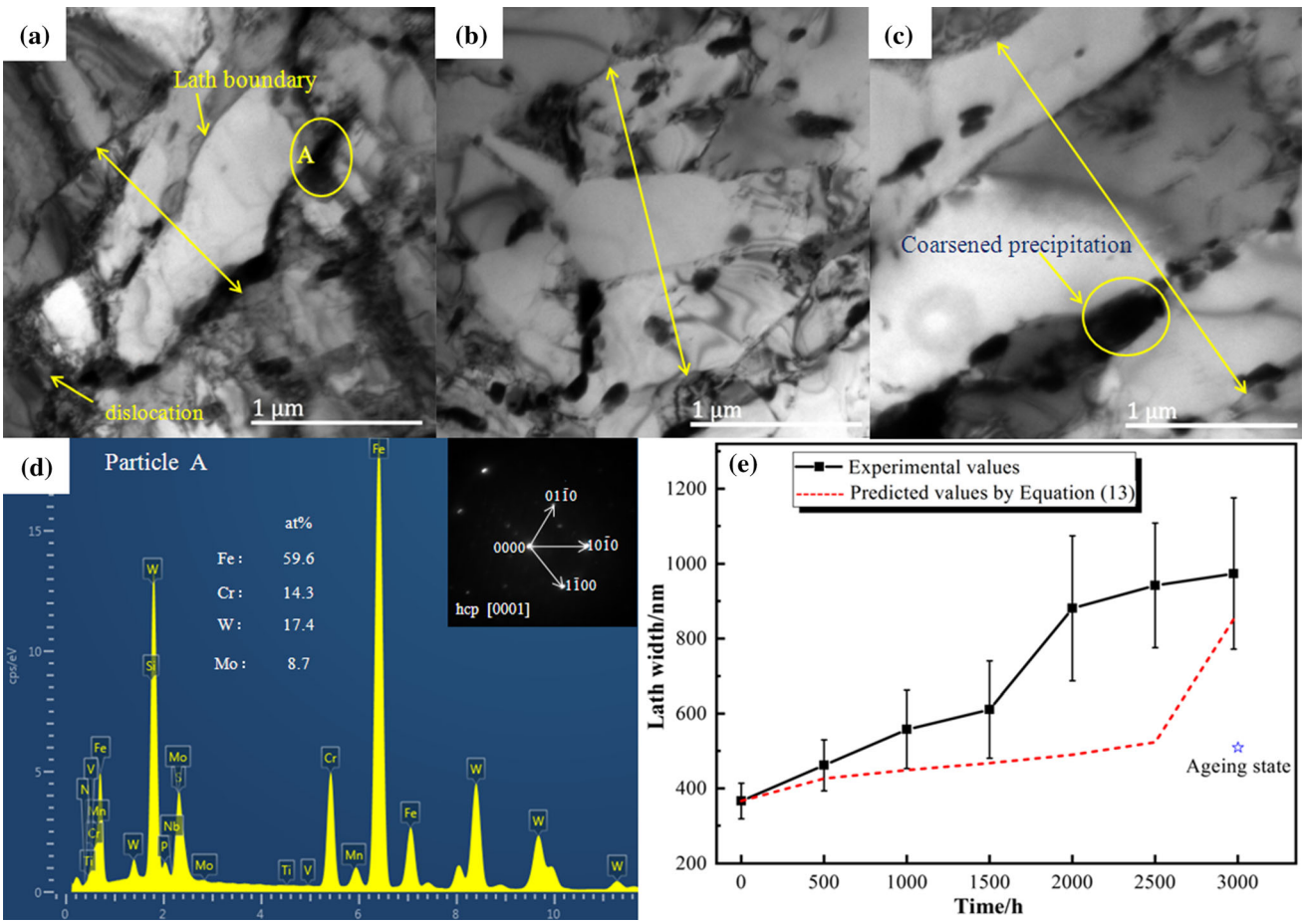

Figure 4 Microstructure evolution at 873 K and 160 MPa: **a** 500 h, **b** 1500 h, **c** 2500 h, **d** EDS and SAED of Laves phase, **e** variation of lath width with creep time.

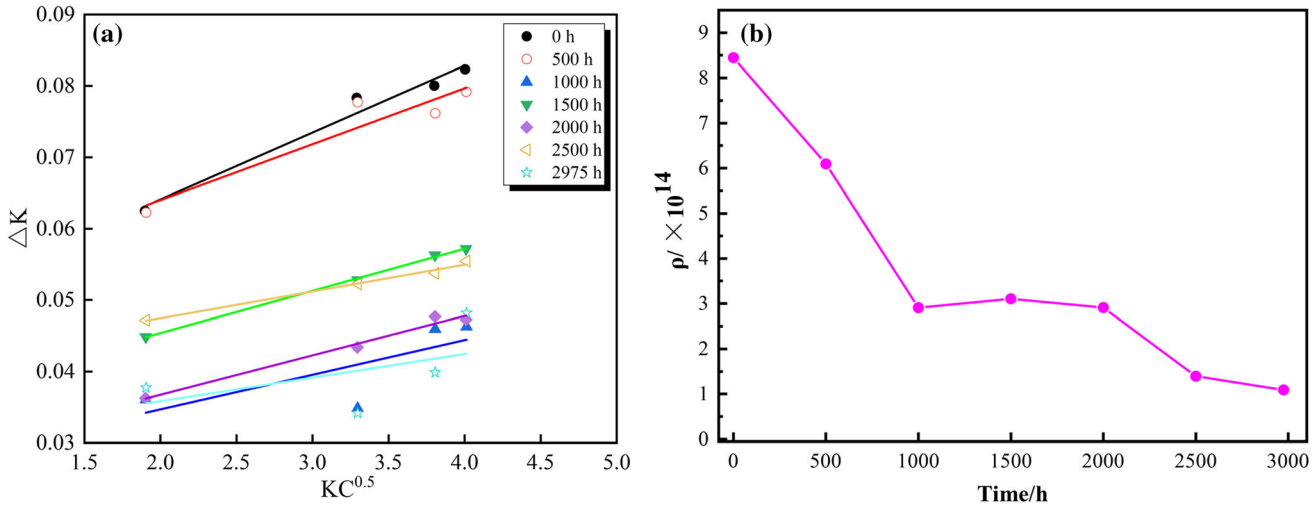

Figure 5 Dislocation density evolution at 873 K and 160 MPa: **a** Modified Williamson-Hall plots and **b** Dislocation density evolution.

angle and the integral breadth of the diffraction peak, C is the average contrast factor of the dislocations for a particular reflection, which can be referred to Ungár [31] and Xu [32]. The as-tempered specimen showed a high dislocation density of 8.4×10^{14} m^{-2}. During the primary creep stage, the dislocation density decreased sharply. Then it almost kept constant in secondary creep stage. Finally, the dislocation density declined to 1.1×10^{14} m^{-2} in tertiary creep stage until creep rupture, which is consistent with the results of Dudko et al. [26], in which the microstructure evolution of a P92-type steel at 650 °C and 118 MPa was investigated.

Coarsening of precipitates

Precipitates play an important role in creep strength of 9% Cr heat-resistant steel due to its retardation effect for movement of dislocations and boundaries [24]. Apart from MX carbonitrides and $M_{23}C_6$ carbides mentioned in sub-Sect. "Microstructure and creep deformation behavior of as-received material", Laves phase precipitates nucleated along boundaries [39] after shortest creep duration at 500 h, as shown in Fig. 4a and d.

The evolution of fractions and size of precipitates with creep time is illustrated in Fig. 6a and b, respectively. The area fraction and size of precipitates within laths such as MX carbonitrides and $M_{23}C_6$ carbides kept almost stable in the whole creep duration, while those located at the boundaries coarsened consistently. The area fraction of $M_{23}C_6$ carbides in boundaries kept stable around 2.8% in the whole creep duration, while the area fraction of Laves phase increased continuously to about 2% at 1500 h and then increased slightly until rupture [40]. The size of the $M_{23}C_6$ carbides and Laves phase increased gradually in the creep duration and did not reach a stable size until rupture. There were some studies reported that Z-phase formation after long-term service in 9–12% Cr steels [13, 14, 22]. Hald reported the precipitation of Z-phase after 30,000 ~ 40,000 h at 923 K [4]. However, no Z-phase was observed in present investigation. This is probably due to inadequate creep duration.

Crystallographic texture and grain boundary characteristic evolution

EBSD analysis of the 9% Cr steels in the as-received state and crept specimen at 873 K and 160 MPa for different creep duration are depicted in Fig. 7. The inverse pole figure(IPF) maps in Fig. 7a–c show that tempered martensite structure retained its original martensite morphology with blocks and packets after creep, and there was insignificant change of texture during the creep. Grain boundary maps overlaid on the image quality maps are depicted in Fig. 7d–f and a statistical comparison is shown in Fig. 7g. It could be observed that the distribution and relative frequency of the low-angle boundaries ($2° \geq \theta < 15°$) and high-angle boundaries ($\theta \geq 15°$) almost kept stable from initial state to rupture state, indicating there was no significant change of grain boundary characteristic during creep.

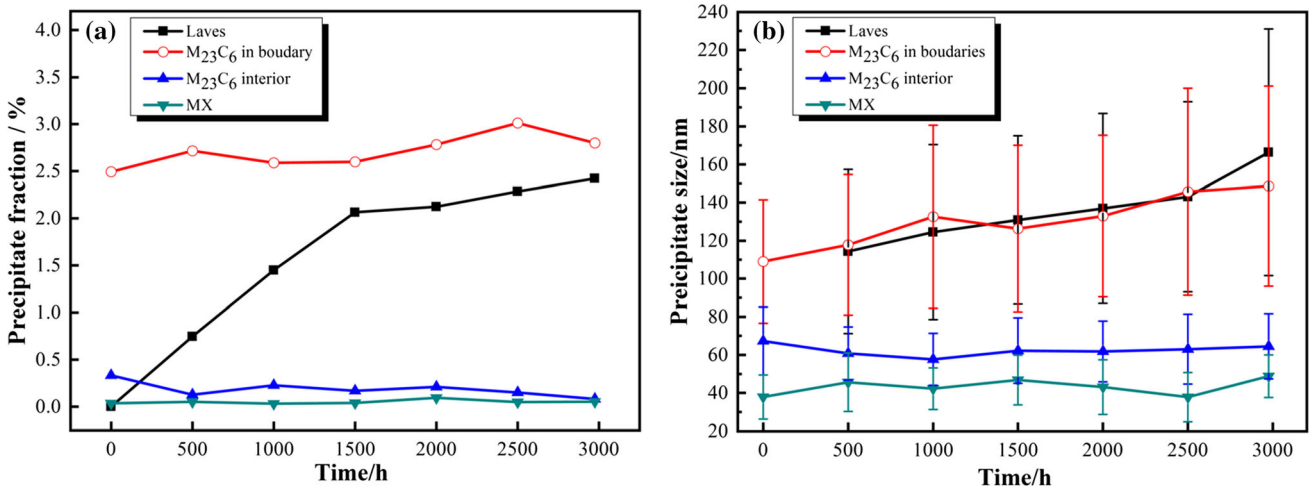

Figure 6 The evolution of **a** precipitates fractions and **b** precipatates size with creep time.

Mechanical properties of interrupted creep specimens

Micro-hardness

Micro-hardness is usually used as an indication of creep life fraction in engineering practices. The micro-hardness of 9% Cr steel at different creep damage condition is shown in Fig. 8. The micro-hardness of gripping and gauge section decreased with the increase in creep time. However, micro-hardness of gauge section declined significantly during the initial creep time of 1000 h and then kept stable to 1500 h creep duration, followed by a continuous decreasing to the end stage. By comparison, the gripping section showed a negligible hardness change during the whole creep time. The different evolutions of hardness in gripping and gauge section indicated that stress exerted more remarkable influences on microstructure evolutions than high-temperature exposure alone, which is consistent with the results reported by other researchers [22, 23].

Tensile properties

The residual high-temperature strength is a key indicator for service parts. The high-temperature mechanical properties of the 9% Cr steels under as-received and different creep conditions are shown in Fig. 9. Figure 9a shows the evolution of 0.2% offset yield strength and ultimate strength at 873 K during creep period. Compared with the as-received material, both yield strength and ultimate tensile strength decreased continuously with the increase in the creep time and did not reach a stable stage until the final stage of the creep. However, the degradation of the strength turned to be relatively stable from 1000 to 1500 h. Different from the monotonous drop of strength properties with the creep time, it was noted that the variation of the ductility properties after different creep duration was relatively negligible, as shown in Fig. 9b.

Fractography observation of tensile specimen

The SEM micrographs of tensile fractured surface for specimens exposed to different creep time are shown in Fig. 10. It can be seen that the fracture morphology mainly consists of the dimples, which are typical characteristics of the transgranular ductile fracture [41]. However, no significant difference can be observed between the fracture surfaces of samples with different creep duration, which is consistent with the negligible variation of elongation.

Discussion

Mechanical property degradation

Micro-hardness

As the creep proceeds, the micro-hardness evolution of 9% Cr steel is mainly attributed to the change of solid-solution hardening, martensite lath width, dislocation density, and precipitation hardening [42].

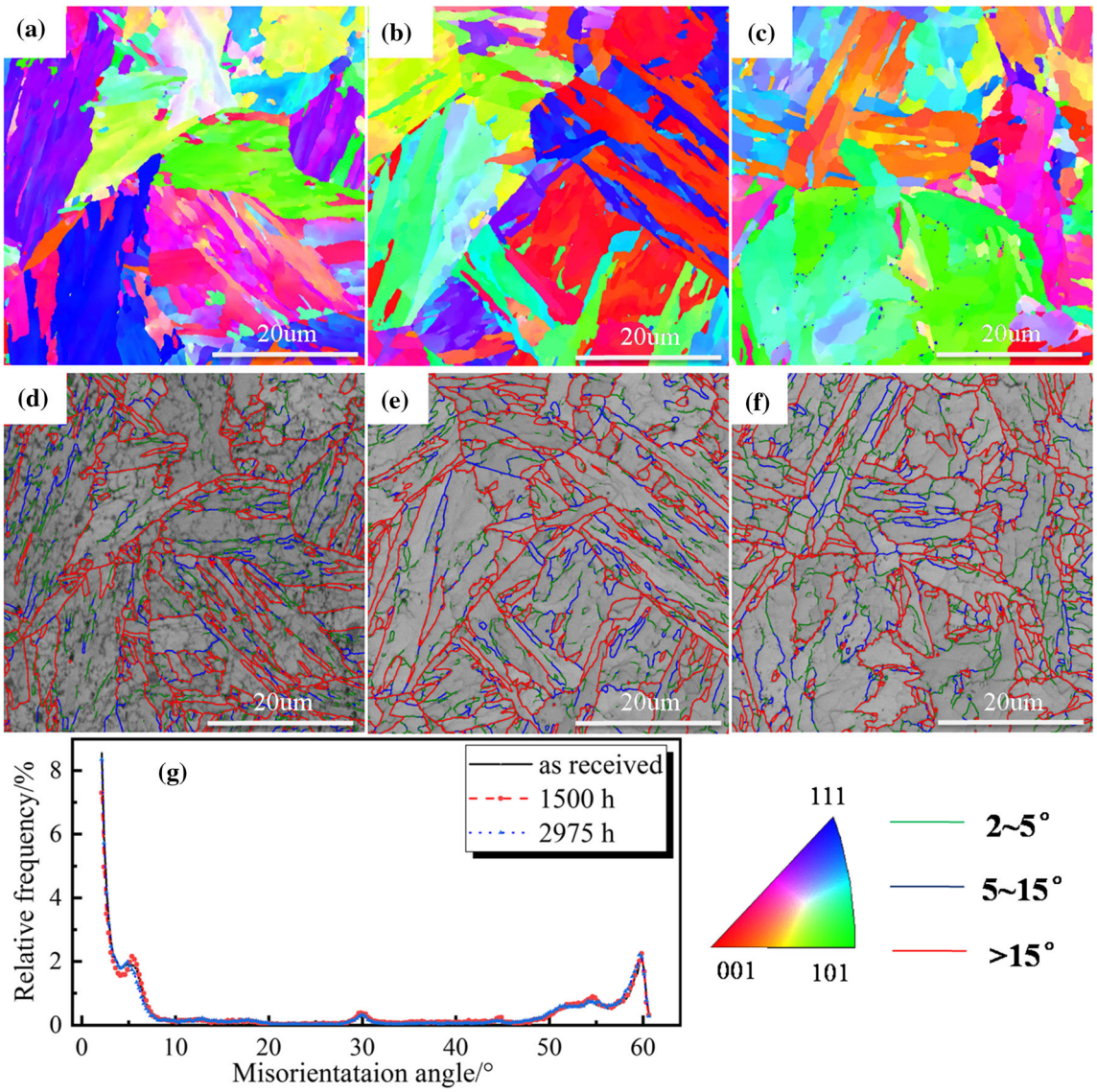

Figure 7 Microstructure evolution of 9% Cr steel with creep lifetime: **a–c**: IPF map of as-received state, 1500 h and 2975 h, respectively, **d–f**: image quality maps with specific grain boundaries of as-received state, 1500 h and 2975 h, respectively, **g**: Relative frequency of misorientation angle.

However, due to the negligible change of the precipitates and solid-solution alloy element distribution during the initial 3000 h of creep, the effect of solid-solution and precipitation hardening on the hardness of 9% Cr steel was insignificant [43]. The reduction in dislocation density and increase in martensite lath may be the major factors for micro-hardness evolution [42]. Sawada et al. [44] pointed that the decrease in dislocation density caused the decline in hardness for modified 9% Cr steel, and the contribution of dislocation on hardness values can be represented as [45]:

$$H_{\mathrm{vp}} = \alpha_{\rho}\, \mathrm{Gb}\, \sqrt{\rho} \tag{1}$$

where H_{vp} is contribution of the dislocation strengthening to the micro-hardness, α_{ρ} is constant, G is the shear modulus, b is the Burger's vector (0.248 nm for ferrite), and ρ is dislocation density.

Armaki [46] proposed that hardness was linearly dependent with the reciprocal of martensite lath width during creep duration. The correlation between them can be expressed as:

$$H_{\mathrm{vl}} = \alpha_{\lambda} \bullet \lambda_{l}^{-1} \tag{2}$$

where H_{vl} is contribution of the martensite lath strengthening to the micro-hardness, α_λ is constant, and λ_l is martensite lath width.

So, Vickers hardness can be described as:

$$H_v = H_{vp} + H_{vl} + H_0 = \alpha_\rho Gb\sqrt{\rho} + \alpha_\lambda \bullet \lambda_l^{-1} + H_0 \quad (3)$$

where H_0 is contribution of matrix, solid solution atoms, and precipitates strengthening to the micro-hardness.

The parameters $\alpha_\rho = 0.51$, $\alpha_\lambda = 5.97$, $H_0 = 179$ were fitted through the experiment data via least square method. The fitted curve through equation was also plotted in contrast to measured value in Fig. 11a. The evolutions of measured value were in good agreement with the fitted curve, suggesting that the microstructure and micro-hardness can be well correlated through Eq. (3). The reduction in dislocation density and increase in martensite lath width were the main factors causing the decline of hardness in the present investigation.

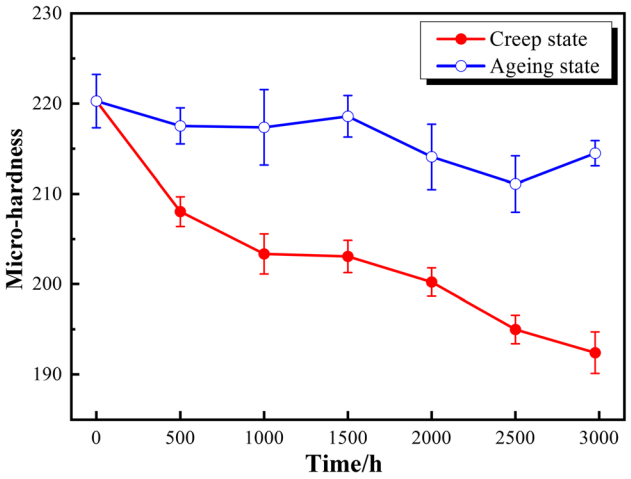

Figure 8 Variation of micro-hardness 9% Cr steels at different lifetime.

High-temperature yield strength

The yield strength of metallic alloy can be divided into two aspects [47, 48]: (i) the contribution of dislocations in the metals, τ_ρ; (ii) the strength provided by obstacle such as boundaries and particles, τ_O. The yield strength can be described as [49]:

$$\sigma_Y = \sqrt{(\tau_\rho^2 + \tau_O^2)} \quad (4)$$

The contribution of dislocation strengthening is described as:

$$\tau_\rho = \alpha_1 \, \mathrm{MGb}\sqrt{\rho} \quad (5)$$

where M is the Taylor factor($\sim$ 3 for bcc iron [50]) and α_1 is a material constant between 0.2 and 0.5.

The contribution of obstacles is defined as:

$$\tau_O = \tau_P + \tau_B + \tau_{PN} + \tau_S + \tau_I \quad (6)$$

where τ_P is the strengthening due to precipitates, τ_B is the contribution of boundaries, τ_{PN} is the Peierls–Nabarro stress, and τ_S and τ_I are the strength provided by solute atoms and interstitial atoms.

The Peierls-Nabarro stress is the shear stress required to move a dislocation in the absence of other strengthening mechanisms, and the Nabarro model is used here.

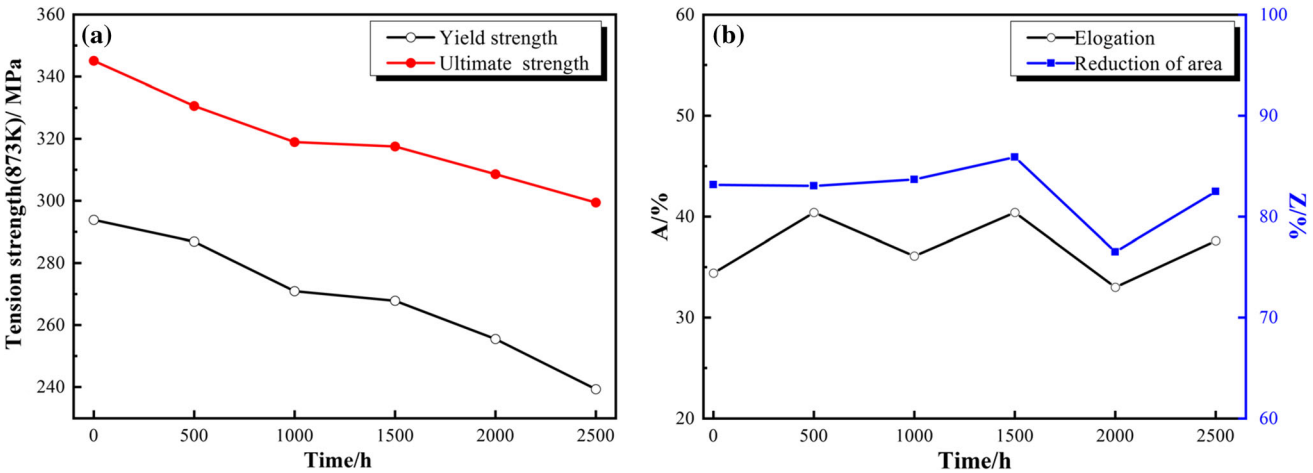

Figure 9 Variation of the **a** yield strength and ultimate strength and **b** elongation and reduction of area at 873 K with different creep time.

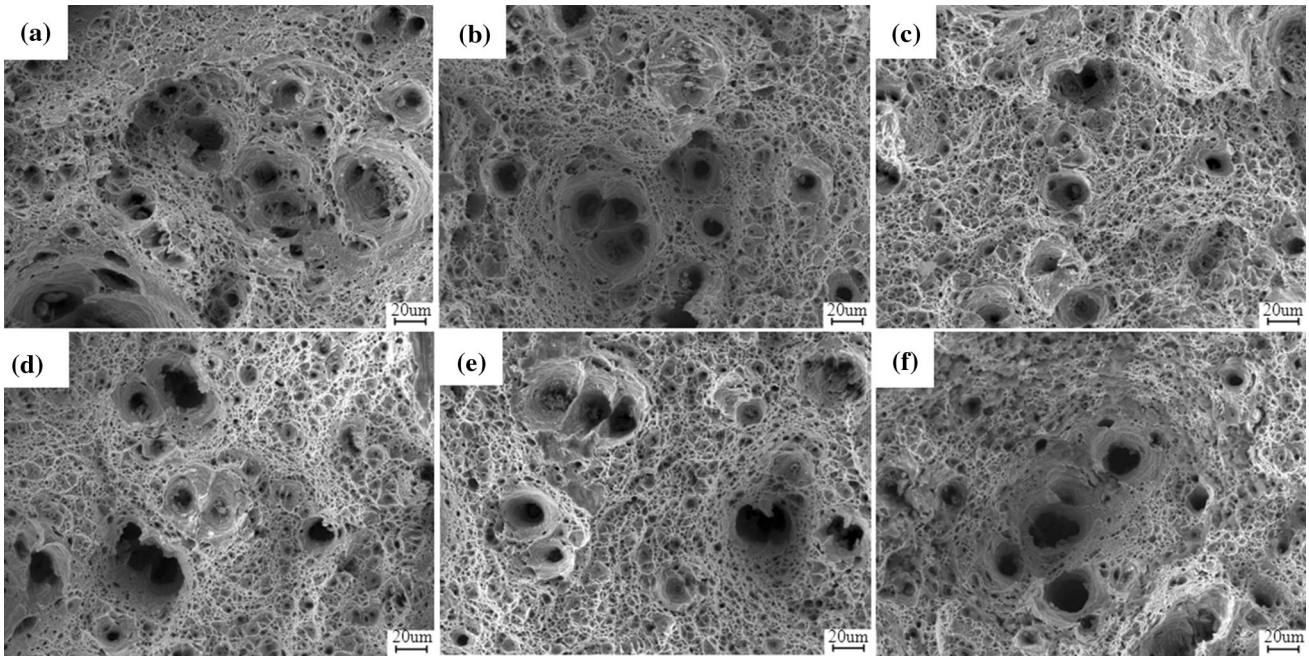

Figure 10 Fractography of tensile specimen exposed to different creep time (873 K,160 MPa): **a** 0 h, **b** 500 h, **c** 1000 h, **d** 1500 h, **e** 2000 h, **f** 2500 h.

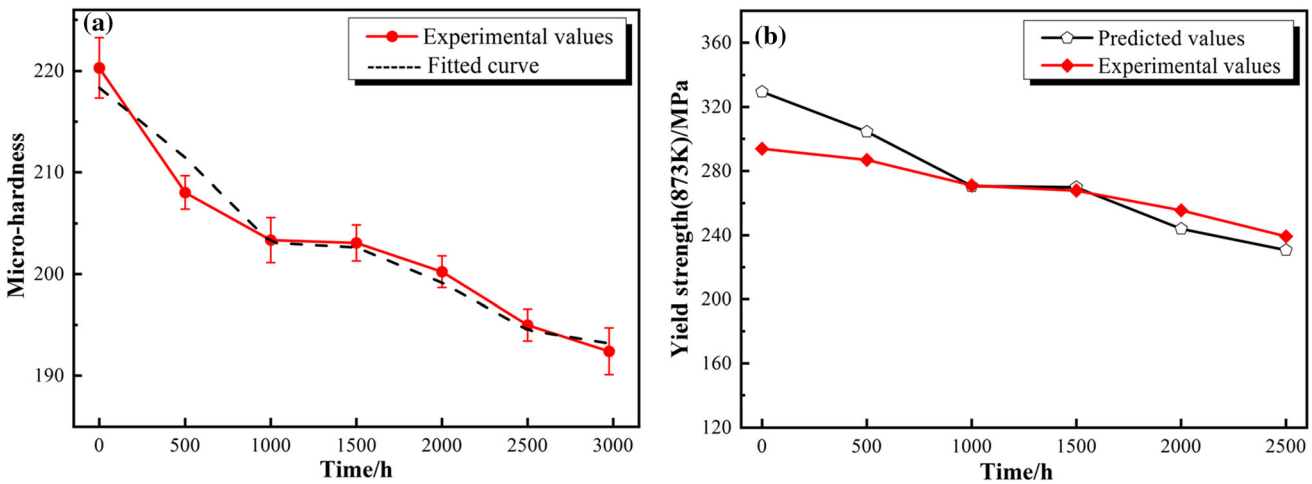

Figure 11 Comparison of experimental values and predicted data: **a** micro-hardness and **b** high-temperature yield strength.

$$\tau_{PN} = \frac{2G}{1-v}\exp\left(\frac{2\pi}{1-v}\right) \tag{7}$$

where v is Poisson's ratio.

The overall contributions of GBs can be expressed as

$$\tau_B = \tau_{HP} + \tau_{LAB} \tag{8}$$

The contribution of HAGB is [51]:

$$\tau_{HP} = \frac{k_{HP}(T)}{\sqrt{d_g}} = \frac{k_{HP(0)}}{\sqrt{d_g}}\exp\left(\frac{-T}{326\,K}\right) \tag{9}$$

where $k_{HP(0)}$ is the Hall–Petch constant at 0 K, d_g is the mean block width.

The contribution of low-angle boundaries is:

$$\tau_{LAB} = \alpha_2\,Gb/\lambda_l \tag{10}$$

where α_2 is a material constant between 2 and 3.

As mentioned before, MX and $M_{23}C_6$ were observed in the as-received materials. MX mainly precipitated in the lath, whereas $M_{23}C_6$ carbide precipitated at both boundaries and interior. Laves phase mainly precipitated on the lath boundaries and

PAGBs. These precipitates not only contribute to the high-temperature strength, but also effectively inhibit the dislocation movement and lath coarsening due to strong pinning effect, thus improve the creep strength.

The contribution of the precipitates can be defined as:

$$\tau_{P,i} = 0.8\,\mathrm{MGb}/\lambda^{p} \tag{11}$$

$$\tau_{P} = f_B\,\tau_{P,B}^{M_{23}C_{6B},\,\mathrm{Laves}} + (1-f_B)\,\tau_{P,\mathrm{IN}}^{\mathrm{MX},\,M_{23}C_{6\mathrm{IN}}} \tag{12}$$

where $\tau_{P,\mathrm{IN}}^{\mathrm{MX},\,M_{23}C_{6\mathrm{IN}}}$ and $\tau_{P,B}^{M_{23}C_{6B},\,\mathrm{Laves}}$ represent precipitates yield strength in the lath interiors and boundaries, respectively, f_B is the fraction of the precipitates located in the boundaries, λ^{p} is mean spacing between precipitates can be expressed as $\lambda^{p} = \sqrt{1/N_i}$, where N_i is the number density of precipitates.

It has been reported that τ_S and τ_I were negligible in previous research [37], so τ_S and τ_I were not taken into consideration in this study. The microstructure parameters are indicated in Table 2. Comparisons between experimental values and predicted yield strength from Eq. (4) are depicted in Fig. 11b.

Microstructure evolution of 9% Cr steels at different creep stage

As mentioned before, decline of dislocation density, recovery of martensite laths, precipitation of new phases and coarsening of precipitates occurred during creep, and quantitatively estimated strengthening contribution at different stage are illustrated in Fig. 12 according to the equations in sub-Sect. "High-temperature yield strength". In this section, the specific role of each factor to the different creep stages will be discussed.

Table 2 Microstructure parameters of 9% Cr steels under different creep life

Creep time (h)	0	500	1000	1500	2000	2500	2975
ρ (10^{14}/m^2)	8.4	6.1	2.9	3.1	2.9	1.4	1.1
λ_l(nm)	366	461	557	610	780	942	974
f_B	0.87	0.95	0.94	0.96	0.94	0.96	0.98
$\lambda^{p}_{\text{(boundaries)}}$	612	558	571	539	539	556	607
$\lambda^{p}_{\text{(interior)}}$	954	1178	955	1070	889	1075	1566

Primary creep stage

In primary creep stage from initial state to about 1000 h, the dislocation density decreased significantly from 8.4×10^{14} m^{-2} to about 2.9×10^{14} m$-^{2}$. The sharp decline of dislocation density during the primary creep stage was mainly attributed to remarkable annihilation of lattice dislocations with opposite signs [52]. Negligible change occurred in size and area fraction of MX carbonitrides by TEM observation, which is consistent with the experimental results observed by Panait et al. [23]. They ascribed that the amount, size and shape of MX carbonitrides kept almost unchanged even after 113, 431 h creep time at 873 K. $M_{23}C_6$ carbides distributed in the intra-lath region also kept stable, and $M_{23}C_6$ carbides located at boundaries coarsened slightly. The fraction of Laves phase increased consistently, but the size remained relative small. In summary, coarsening of precipitates was negligible in this stage. Although fine precipitates dispersed in the matrix and boundaries provided strong pinning force to the migration of lath boundaries, the coarsening of martensite lath was also appreciable, as shown in Fig. 4. These may attributed to the high creep stress in this study. So, as illustrated in Fig. 13b, the degradation of micro-hardness and strength was mainly attributed to the decline of dislocation density and coarsening of martensite lath, which can also be verified by quantitative analysis in Fig. 12.

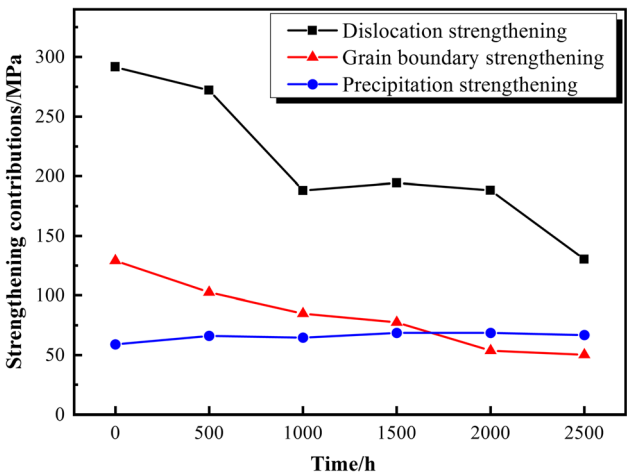

Figure 12 The strengthening contribution of dislocation, grain boundary, and precipitation at different creep stages.

Secondary creep stage

During elevated temperature deformation, martensite lath boundaries act as both sources and sinks for dislocations and play an important role in plastic deformation [53]. In the secondary creep stage from about 1000 to 2000 h, the increase in lattice dislocations resulted from knitting out of lath boundaries was in balance with the decrease in dislocation trapped by the boundaries, and hence the overall dislocation density kept stable [52]. The coarsening of precipitates was still sluggish. The predominant microstructure change in this stage was probably the widening of martensite lath, as shown in Fig. 12.

Abe [54] proposed two mechanisms for coarsening of martensite lath, the combination of two adjacent laths and the movement of the Y-junctions. The combination of two lath boundaries will generally cause the disappearance of lath boundaries, leaving the row of $M_{23}C_6$ carbides in the matrix. However, there was no overwhelming evidence to verify the presence of the row of precipitates in the present research, which is in consistent with previous research [54, 55]. As a result, it can be inferred that the movement of Y-junctions underlying the lath coarsening was the main mechanism for the coarsening of martensite lath in the present study, as illustrated in Fig. 13c. Martensite laths hardly coarsened under stress-free state for 3% Co modified P92 steel [56, 57], and applied stress played an important role in martensite lath coarsening [23, 43, 58], which also can be confirmed in this study (Fig. 4e). Qin [59] have proposed a model to clarify the relationship between the subgrain size and applied stress (σ),

$$\log \lambda_l = \log \lambda_s + \log\left(\frac{\lambda_0}{\lambda_s}\right) exp\left(\frac{-\varepsilon}{k\,(\sigma)}\right) \tag{13}$$

where λ_l represents the subgrain size, λ_0 is the subgrain size for as-received specimen, $k(\sigma) \approx 0.12$ is a growth constant, $\lambda_s = 10Gb/\sigma$ is subgrain size in the steady-state [60], G is shear modulus at given temperature, and ε is the accumulated creep strain.

The comparisons of the measured results and calculated lath width using Eq. (13) are shown in Fig. 4e. The measured results are consistent with the experimental results of Xiao et al. [37], whereas experimental data were slightly higher than predicted values [23]. Armaki et al. [36] reported that coarsening of martensite lath was controlled by strain in short-term creep regime, but controlled by the stability of precipitates during long-term creep. Aghajani [43] has verified that the subgrain widths were well rationalized and predicted by Eq. (13) for long-term creep test under relative low creep stress. The deviation of the experimental and modeling results here was probably because the fact that the interrupted tests were conducted under high creep stress, in which regime the coarsening of the lath was mainly controlled by strain rather than the stability of precipitates. Besides, it is possible to estimate the

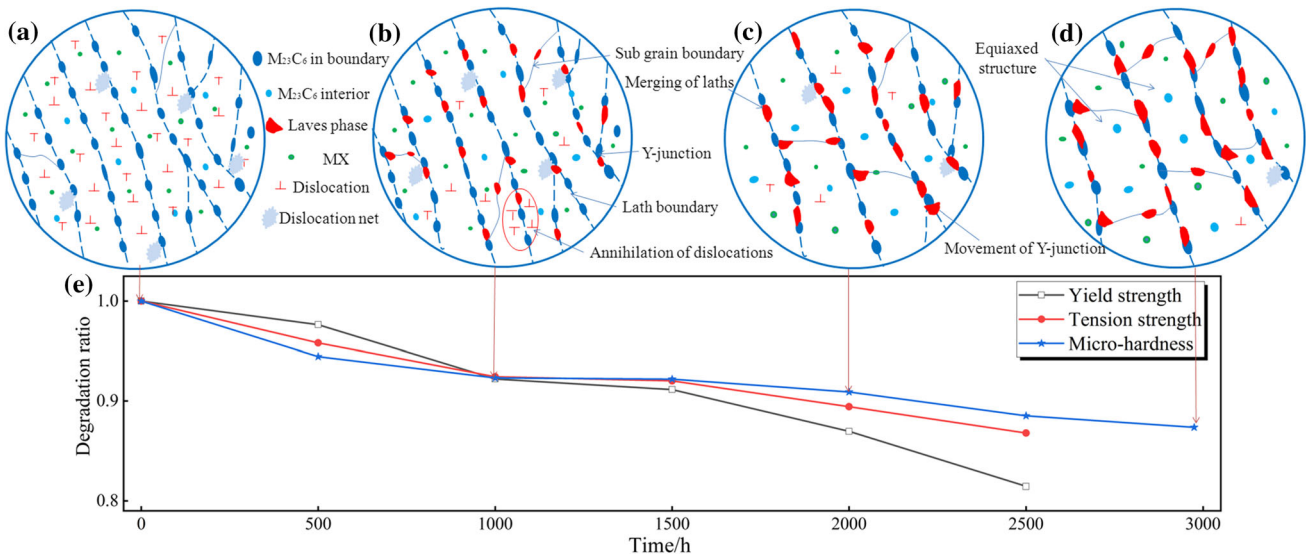

Figure 13 Schematic diagram of microstructure evolution at different creep stage: **a** initial state, **b** 1000 h, **c** 2000 h, **d** 2975 h, **e** degradation trend.

accumulated creep strain via the actual subgrain size based on the relationship depicted in Eq. (13). In turn, the creep strain and residual lifetime also can be predicted by the subgrain size [61].

Tertiary creep stage

It was widely accepted that $M_{23}C_6$ carbides play more effective role on hindering the coarsening of martensite lath than MX carbonitrides and Laves phase. The carbide-stabilized substructure strengthening was the most significant contribution on the creep strength [36, 62–65]. The coarsening rate of $M_{23}C_6$ carbides in the boundaries was obviously higher than interior for the solute atoms diffused faster in the boundaries. Creep strain can also accelerate the coarsening of $M_{23}C_6$ carbides; this is probably because solution atoms diffused faster under creep condition [66, 67]. In the meantime, Laves phase coarsened consistently after nucleation, as shown in Fig. 6.

The continuous coarsening of precipitates not only reduced the precipitation strengthening but also mitigated the interaction between free dislocation and boundaries. When the pinning force between precipitates and boundaries dropped below a critical value, the boundaries will detach from precipitates [26, 68]. Then the movement and merging of martensite lath were no longer suppressed, leading to the quick recovery of martensite lath structure. The disappearance of some lath boundaries and increase in lath width highly facilitated dislocation glide and contributed to further reduction in dislocation, especially the low-angle boundaries. The continuous decline of the dislocation density lowered the drag effect between dislocation and solution atom, thus promoted the further coarsening of precipitates. Then the process trapped into a vicious circle, resulting in the continuous degradation of 9% Cr steels. A schematic illustration of the synergistic effect of coarsening of martensite lath and precipitates and decline of dislocation density occurred in the tertiary creep stage, as illustrated in Figs. 12 and 13d.

The role of Laves phase during creep

It was reported that Laves phase nucleated at the PAGBs or martensite lath boundaries, as well as the position adjacent to $M_{23}C_6$ carbides [11, 69, 70]. Precipitation of Laves phase depleted W and Mo from solid solution, thus decreased the solution strengthening [29]. On the other hand, finely dispersed Laves phase in early stage can also provide precipitation strengthening [71]. It was interesting to find that although the dislocation density kept stable and martensite laths continued to coarsen from 1000 to 1500 h, the strength exhibited insignificant degradation. This is probably due to that the continuous precipitation of dispersed fine Laves phase compensated for the coarsening effect. As depicted in Fig. 12, the contributions of dislocation strengthening and grain boundary strengthening declined while the precipitation strengthening increased. Wang et al. [72] reported that Laves phase particles nucleated rapidly within the first approximately 1500 h during aging and then coarsened significantly after about 3000 h. Consistent nucleation of fine Laves phase decreased the mean space between the precipitates on the boundaries, hence exerted additional pining force for migrating boundaries and dislocations [73]. In the present research, the average size of Laves phase at rupture state coarsened to only 166 nm, which was similar to $M_{23}C_6$ carbides. As shown in Fig. 14a, dispersed Laves phase particles distributed at boundaries hindered the movement of dislocation and boundaries, thus contributing to precipitation strengthening and lath (subgrain) strengthening.

Xu et al. [32] have reported obvious strain concentration around large Laves phase, which deteriorated mechanical properties, especially ductility. In order to better characterize the strain distribution around Laves phase, TKD examination with EDS mapping was conducted with rupture specimen at 2975 h. Forward scattered image corresponding to TEM micrograph is shown in Fig. 14b, and image quality and phase map are depicted in Fig. 14c, and mapping images of Cr, W and Mo are depicted in Fig. 14e and f, respectively. From these, we can clearly distinguish the distribution of $M_{23}C_6$ carbides and Laves phase in matrix by element mapping images. Kernel average misorientation (KAM) analysis for 9% Cr steel shown in Fig. 14d indicated insignificant strain concentration around Laves phase even at rupture state. Lee et al. [18] have reported a critical size of 130 nm for Laves phase triggered the ductile to brittle transition. Coarsened Laves phase particles located at boundaries can hinder plastic deformation and cause stress concentration, which induce creep cavities, reduction of the strength and ductility and brittle intergranular fracture [11]. The

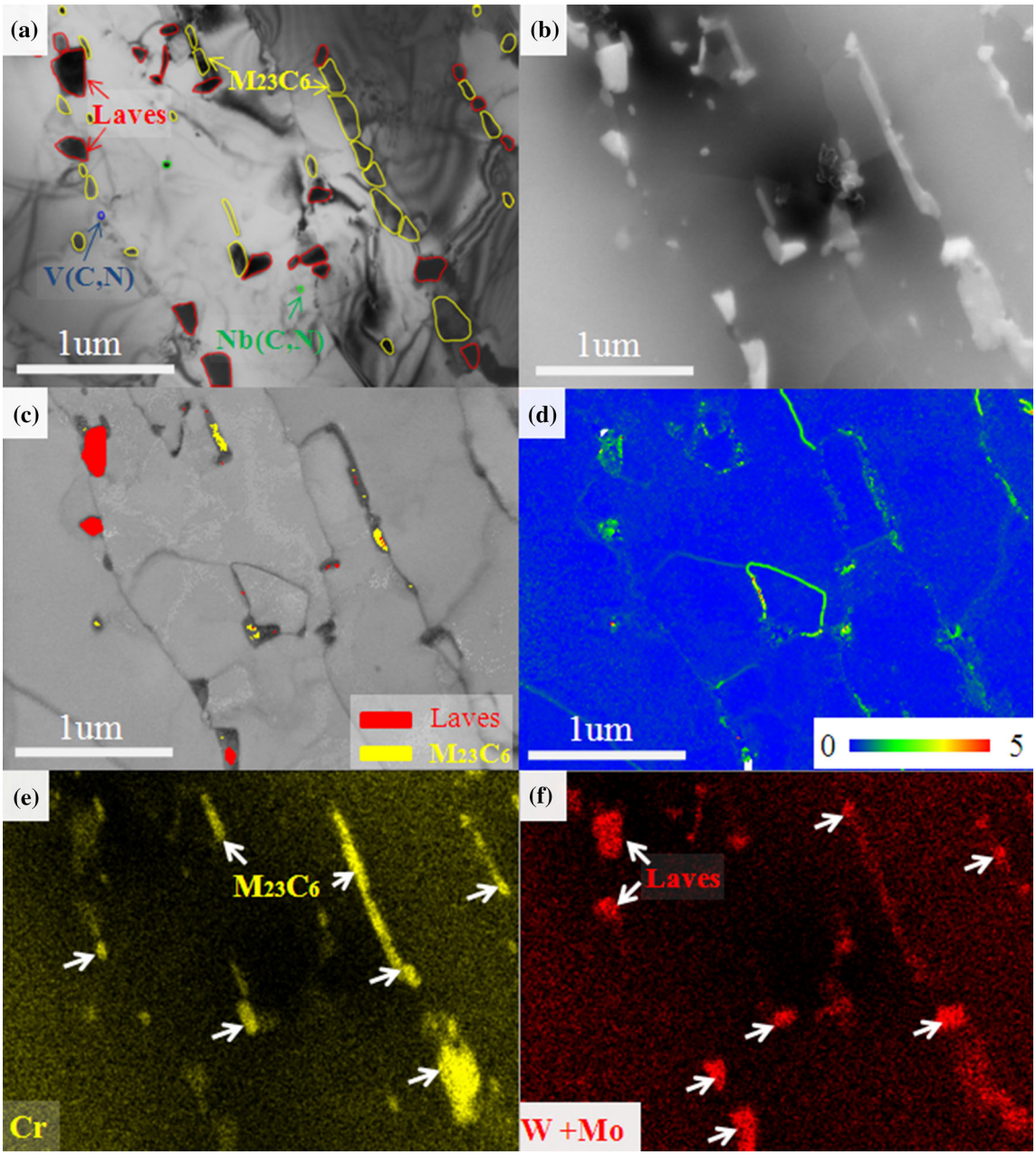

Figure 14 Laves phase in 9% Cr steel at 2975 h (rupture state): **a** TEM micrograph, **b** forward scattered image corresponding to (**a**), **c** image quality and phase map, **d** Kernel average misorientation (KAM) analysis, mapping images of Cr (**e**), W and Mo (**f**).

elongation and fractured morphology of tension specimens exposed to different creep duration basically kept unchanged in the present study, as shown in Figs. 9 and 10. It can be attributed to the relative small size of Laves phase particles dispersed at the boundaries, which provide precipitation strengthening without deteriorating the ductility. The precipitation of Laves phase in early stage provided additional strengthening effect and compensated for the strength loss caused by the coarsening of martensite lath. Moreover, the growth of Laves phase induced insignificant stain concentration and ductility deterioration.

Conclusions

In the present work, the evolutions of mechanical properties and corresponding microstructure during creep were investigated by conducting a series of interrupted creep test in a 9% Cr heat-resistant steels. The relationship between mechanical properties and microstructure evolution was analyzed. The predominant factors for degradation of mechanical properties at different creep stage were discussed. The main conclusions can be drawn from present investigations:

1. The dislocation density declined from 8.4×10^{14} m^{-2} at initial state to 1.1×10^{14} m^{-2} after rupture at 2975 h, while the width of martensite lath increased from 366 to 974 nm. The average size of Laves phase and $M_{23}C_6$ carbides located at boundaries increased from about 110 to around 160 nm, whereas the average size of MX phase and $M_{23}C_6$ carbides within laths kept stable at 43 nm and 62 nm, respectively. No significant change of grain boundary characteristic was found during the creep.
2. The high-temperature yield strength (micro-hardness) significantly decreased from 294 MPa (220 HV0.1) at initial state to 271 MPa (203 HV0.1) at 1000 h and kept relatively stable to 1500 h and then declined continuously to 239 MPa (192 HV0.1) until rupture. The elongation and fractured morphology of tension specimens exposed to different creep duration basically kept unchanged.
3. The main mechanisms for degradation of mechanical properties in primary creep stage were decline of dislocation density and coarsening of martensite lath. Coarsening of martensite lath, as well as precipitation strengthening played significant role in secondary creep stage. In tertiary creep stage, synergistic effect of coarsening of martensite lath and precipitates and decline of dislocation density resulted in accelerated degradation of mechanical properties.
4. The precipitation of Laves phase in early stage provided additional strengthening effect and compensated for the strength loss caused by the coarsening of martensite lath, contributing to the stability of mechanical properties from 1000 to 1500 h. Moreover, the growth of Laves phase induced insignificant stain concentration and ductility deterioration.

Acknowledgements

This research did not receive any specific grant from funding agencies in the public, commercial, or not-for-profit sectors.

Author contributions

LMF and ADS designed the study, ZGZ and YFW conducted TEM observation, GQT carried out other experiments and wrote the manuscript, BM and YTX helped to evaluate the data and revised the manuscript.

Data availability

The raw/processed data required to reproduce these findings can be shared if necessary.

Declarations

Conflict of interest The authors declare that they have no conflict of interest.

Ethical approval The experiments in this study were not involved in any human tissue and related issues.

References

[1] Fan H, Zhang Z, Dong J, Xu W (2018) China's R&D of advanced ultra-supercritical coal-fired power generation for addressing climate change. Therm Sci Eng Prog 5:364–371. https://doi.org/10.1016/j.tsep.2018.01.007

[2] Klueh RL (2013) Elevated temperature ferritic and martensitic steels and their application to future nuclear reactors. Int Mater Rev 50:287–310. https://doi.org/10.1179/174328005X41140

[3] Abe F (2008) Precipitate design for creep strengthening of 9% Cr tempered martensitic steel for ultra-supercritical power plants. Sci Technol Adv Mat 9:013002. https://doi.org/10.1088/1468-6996/9/1/013002

[4] Hald J (2008) Microstructure and long-term creep properties of 9–12% Cr steels. Int J Pres Ves Pip 85:30–37. https://doi.org/10.1016/j.ijpvp.2007.06.010

[5] Ennis PJ, Czyrska-Filemonowicz A (2003) Recent advances in creep-resistant steels for power plant applications. Sadhana 28:709–730. https://doi.org/10.1007/BF02706455

[6] Jones DRH (2004) Creep failures of overheated boiler, superheater and reformer tubes. Eng Fail Anal 11:873–893. https://doi.org/10.1016/j.engfailanal.2004.03.001

[7] Pešička J, Kužel R, Dronhofer A, Eggeler G (2003) The evolution of dislocation density during heat treatment and creep of tempered martensite ferritic steels. Acta Mater 51:4847–4862. https://doi.org/10.1016/S1359-6454(03)00324-0

[8] Yadav SD, Kalácska S, Dománková M, Yubero DC, Resel R, Groma I, Beal C, Sonderegger B et al (2016) Evolution of the substructure of a novel 12% Cr steel under creep conditions. Mater Charact 115:23–31. https://doi.org/10.1016/j.matchar.2016.03.015

[9] Ghassemi Armaki H, Chen R, Maruyama K, Igarashi M (2010) Premature creep failure in strength enhanced high Cr ferritic steels caused by static recovery of tempered martensite lath structures. Mater Sci Eng A 527:6581–6588. https://doi.org/10.1016/j.msea.2010.07.037

[10] Ghassemi-Armaki H, Chen RP, Maruyama K, Yoshizawa M, Igarashi M (2009) Static recovery of tempered lath martensite microstructures during long-term aging in 9–12% Cr heat resistant steels. Mater Lett 63:2423–2425. https://doi.org/10.1016/j.matlet.2009.08.024

[11] Maddi L, Deshmukh GS, Ballal AR, Peshwe DR, Paretkar RK, Laha K, Mathew MD (2016) Effect of Laves phase on the creep rupture properties of P92 steel. Mater Sci Eng A 668:215–223. https://doi.org/10.1016/j.msea.2016.05.074

[12] Dimmler G, Weinert P, Kozeschnik E, Cerjak H (2003) Quantification of the Laves phase in advanced 9–12% Cr steels using a standard SEM. Mater Charact 51:341–352. https://doi.org/10.1016/j.matchar.2004.02.003

[13] A G (2006) Z-phase in 9–12% Cr Steels.PhD Dissertation, Technical University of Denmark

[14] Cipolla L, Danielsen HK, Venditti D, Di Nunzio PE, Hald J, Somers MAJ (2010) Conversion of MX nitrides to Z-phase in a martensitic 12% Cr steel. Acta Mater 58:669–679. https://doi.org/10.1016/j.actamat.2009.09.045

[15] Wang Y, Kannan R, Li L (2020) Insight into Type IV cracking in Grade 91 steel weldments. Mater Des 190:108570. https://doi.org/10.1016/j.matdes.2020.108570

[16] Masuyama F, Yamaguchi T(2014). New ferritic steel beyond grade 92 and its creep degradation assessment by hardness method for grade 91. In: ASME 2014 symposium on elevated temperature application of materials for fossil, nuclear, and petrochemical industries: pp 54–61

[17] Mukhopadhyay SK, Roy H, Roy A (2009) Development of hardness-based model for remaining life assessment of thermally loaded components. Int J Pres Ves Pip 86:246–251. https://doi.org/10.1016/j.ijpvp.2008.11.014

[18] Lee JS, Armaki HG, Maruyama K, Muraki T, Asahi H (2006) Causes of breakdown of creep strength in 9Cr–1.8W–0.5Mo–VNb steel. Mater Sci Eng A 428:270–275. https://doi.org/10.1016/j.msea.2006.05.010

[19] Jin X, Zhu B, Li Y, Zhao Y, Xue F, Zhang G (2020) Effect of the microstructure evolution on the high-temperature strength of P92 heat-resistant steel for different service times. Int J Pres Ves Pip 186:104131. https://doi.org/10.1016/j.ijpvp.2020.104131

[20] Xia X, Zhu B, Jin X, Tang M, Yang L, Xue F, Shi J, Zhang G (2021) Analysis on microstructure and properties evolution and life prediction of P92 steel in high temperature service. Int J Pres Ves Pip 194:104482. https://doi.org/10.1016/j.ijpvp.2021.104482

[21] Guo X, Jiang Y, Gong J, Weng X (2016) The influence of long-term thermal exposure on microstructural stabilization and mechanical properties in 9Cr-0.5Mo-1.8W-VNb heat-resistant steel. Mater Sci Eng A 672:194–202. https://doi.org/10.1016/j.msea.2016.07.006

[22] Panait CG, Bendick W, Fuchsmann A, Gourgues-Lorenzon AF, Besson J (2010) Study of the microstructure of the grade 91 steel after more than 100,000 h of creep exposure at 600 °C. Int J Pres Ves Pip 87:326–335. https://doi.org/10.1016/j.ijpvp.2010.03.017

[23] Panait CG, Zielińska-Lipiec A, Koziel T, Czyrska-Filemonowicz A, Gourgues-Lorenzon A-F, Bendick W (2010) Evolution of dislocation density, size of subgrains and MX-type precipitates in a P91 steel during creep and during thermal ageing at 600°C for more than 100,000h. Mater Sci Eng A 527:4062–4069. https://doi.org/10.1016/j.msea.2010.03.010

[24] Nie M, Zhang J, Huang F, Liu JW, Zhu XK, Chen ZL, Ouyang LZ (2014) Microstructure evolution and life assessment of T92 steel during long-term creep. J Alloys Compd 588:348–356. https://doi.org/10.1016/j.jallcom.2013.11.080

[25] Orlová A, Buršık J, Kuchařová K, Sklenička V (1998) Microstructural development during high temperature creep of 9% Cr steel. Mater Sci Eng A 245:39–48. https://doi.org/10.1016/S0921-5093(97)00708-9

[26] Dudko V, Belyakov A, Molodov D, Kaibyshev R (2011) Microstructure evolution and pinning of boundaries by precipitates in a 9 pct Cr heat resistant steel during creep. Metall

Mater Trans A 44:162–172. https://doi.org/10.1007/s11661-011-0899-1

[27] Sawada K, Kushima H, Tabuchi M, Kimura K (2011) Microstructural degradation of Gr.91 steel during creep under low stress. Mater Sci Eng A 528:5511–5518. https://doi.org/10.1016/j.msea.2011.03.073

[28] Tkachev E, Belyakov A, Kaibyshev R (2018) Creep behavior and microstructural evolution of a 9%Cr steel with high B and low N contents. Mater Sci Eng A 725:228–241. https://doi.org/10.1016/j.msea.2018.04.032

[29] Ennis PJ, Zielinska-Lipiec A, Czyrska-Filemonowicz A, Wachter O (1997) Microstructural stability and creep rupture strength of the martensitic steel P92 for advanced power plant. Acta Mater 45:4901–4907. https://doi.org/10.1016/S1359-6454(97)00176-6

[30] Cong Z, Murata Y (2011) Dislocation density of lath martensite in 10Cr-5W heat-resistant steels. Mater Trans JIM 52:2151–2154. https://doi.org/10.2320/matertrans.M2011201

[31] Ungár T, Borbély A (1996) The effect of dislocation contrast on x-ray line broadening: a new approach to line profile analysis. Appl Phys Lett 69:3173–3175. https://doi.org/10.1063/1.117951

[32] Xu Y, Nie Y, Wang M, Li W, Jin X (2017) The effect of microstructure evolution on the mechanical properties of martensite ferritic steel during long-term aging. Acta Mater 131:110–122. https://doi.org/10.1016/j.actamat.2017.03.045

[33] Shrestha T, Basirat M, Charit I, Potirniche GP, Rink KK, Sahaym U (2012) Creep deformation mechanisms in modified 9Cr–1Mo steel. J Nucl Mater 423:110–119. https://doi.org/10.1016/j.jnucmat.2012.01.005

[34] Guguloth K, Roy N (2018) Study on the creep deformation behavior and characterization of 9Cr-1Mo-V-Nb steel at elevated temperatures. Mater Charact 146:279–298. https://doi.org/10.1016/j.matchar.2018.10.011

[35] Maruyama K, Sawada K, Koike J-i (2001) Strengthening mechanisms of creep resistant tempered martensitic steel. ISIJ Int 41:641–653. https://doi.org/10.2355/isijinternational.41.641

[36] Ghassemi Armaki H, Chen R, Maruyama K, Igarashi M (2011) Creep behavior and degradation of subgrain structures pinned by nanoscale precipitates in strength-enhanced 5 to 12 Pct Cr ferritic steels. Metall Mater Trans A 42:3084–3094. https://doi.org/10.1007/s11661-011-0726-8

[37] Xiao B, Xu L, Tang Z, Zhao L, Jing H, Han Y, Li H (2019) A physical-based yield strength model for the microstructural degradation of G115 steel during long-term creep. Mater Sci Eng A 747:161–176. https://doi.org/10.1016/j.msea.2019.01.051

[38] Yadav SD, El-Tahawy M, Kalácska S, Dománková M, Yubero DC, Poletti C (2017) Characterizing dislocation configurations and their evolution during creep of a new 12% Cr steel. Mater Charact 134:387–397. https://doi.org/10.1016/j.matchar.2017.11.017

[39] Xu Y, Wang M, Wang Y, Gu T, Chen L, Zhou X, Ma Q, Liu Y et al (2015) Study on the nucleation and growth of Laves phase in a 10% Cr martensite ferritic steel after long-term aging. J Alloys Compd 621:93–98. https://doi.org/10.1016/j.jallcom.2014.09.204

[40] Gururaj K, Pal S (2019) Influence of dislocation density and grain size on precipitation kinetics on P92 grade steel. Mater Today 18:1364–1374. https://doi.org/10.1016/j.matpr.2019.06.602

[41] Sklenicka V, Kucharova K, Svobodova M, Kral P, Kvapilova M, Dvorak J (2018) The effect of a prior short-term ageing on mechanical and creep properties of P92 steel. Mater Charact 136:388–397. https://doi.org/10.1016/j.matchar.2018.01.008

[42] Masuyama F (2009) Hardness model for creep-life assessment of high-strength martensitic steels. Mater Sci Eng A 510–511:154–157. https://doi.org/10.1016/j.msea.2008.04.133

[43] Aghajani A (2009) Evolution of microstructure during long-term creep of a tempered martensite ferritic steel.PhD Dissertation, Ruhr University Bochum

[44] Sawada K, Miyahara K, Kushima H, Kimura K, Matsuoka S (2005) Contribution of microstructural factors to hardness change during creep exposure in Mod. 9Cr-1Mo steel. ISIJ Int 45:1934–1939. https://doi.org/10.2355/isijinternational.45.1934

[45] Zhu L (2019) Creep behavior and life prediction of high chromium heat resistant steel at elevated temperature PhD Dissertation, Northwest University

[46] Ghassemi-Armaki H, Chen RP, Maruyama K, Igarashi M (2013) Contribution of recovery mechanisms of microstructure during long-term creep of Gr.91 steels. J Nucl Mater 433:23–29. https://doi.org/10.1016/j.jnucmat.2012.09.026

[47] Kocks UF, Argon AS, Ashby MF (1975) Thermodynamics and kinetics of slip. Pergamon press, Oxford

[48] Nikitin I (2020) Strengthening mechanisms of creep-resistant 12%Cr–3%Co steel with low N and high B contents. J Mater Sci 55:7530–7545. https://doi.org/10.1007/s10853-020-04508-7

[49] Li Q (2003) Modeling the microstructure–mechanical property relationship for a 12Cr–2W–V–Mo–Ni power plant steel. Mater Sci Eng A 361:385–391. https://doi.org/10.1016/S0921-5093(03)00565-3

[50] Rosenberg JM, Piehler HR (1971) Calculation of the taylor factor and lattice rotations for bcc metals deforming by pencil glide. Metall Trans 2:257–259. https://doi.org/10.1007/BF02662666

[51] Barrett RA, O'Donoghue PE, Leen SB (2018) A physically-based high temperature yield strength model for 9Cr steels. Mater Sci Eng A 730:410–424. https://doi.org/10.1016/j.msea.2018.05.086

[52] Dudko V, Belyakov A, Kaibyshev R (2016) Evolution of lath substructure and internal stresses in a 9% Cr steel during creep. ISIJ Int Advpub. https://doi.org/10.2355/isijinternational.ISIJINT-2016-334

[53] Mitsuhara M, Yamasaki S, Miake M, Nakashima H, Nishida M, Kusumoto J, Kanaya A (2016) Creep strengthening by lath boundaries in 9Cr ferritic heat-resistant steel. Philos Mag Lett 96:76–83. https://doi.org/10.1080/09500839.2016.1154200

[54] Abe F (2004) Coarsening behavior of lath and its effect on creep rates in tempered martensitic 9Cr–W steels. Mater Sci Eng A 387–389:565–569. https://doi.org/10.1016/j.msea.2004.01.057

[55] Xu L, Zhang D, Liu Y, Ning B, Qiao Z, Yan Z, Li H (2014) Precipitation behavior and martensite lath coarsening during tempering of T/P92 ferritic heat-resistant steel. Int J Miner Metall Mater 21:438–447. https://doi.org/10.1007/s12613-014-0927-4

[56] Fedoseeva A, Dudova N, Kaibyshev R (2016) Creep strength breakdown and microstructure evolution in a 3%Co modified P92 steel. Mater Sci Eng A 654:1–12. https://doi.org/10.1016/j.msea.2015.12.027

[57] Sawada K, Maruyama K, Hasegawa Y, Muraki T (1999) Creep life assessment of high chromium ferritic steels by Recovery of martensitic lath structure. Key Eng Mater 171–174:109–114. https://doi.org/10.4028/www.scientific.net/KEM.171-174.109

[58] Sawada K, Taneike M, Kimura K, Abe F (2003) In situ observation of recovery of lath structure in 9% chromium creep resistant steel. Mater Sci Technol 19:739–742. https://doi.org/10.1179/026708303225010696

[59] Qin Y, Götz G, Blum W (2003) Subgrain structure during annealing and creep of the cast martensitic Cr-steel G-X12CrMoWVNbN 10–1-1. Mater Sci Eng A 341:211–215. https://doi.org/10.1016/S0921-5093(02)00215-0

[60] Sawada K, Takeda M, Maruyama K, Ishii R, Yamada M, Nagae Y, Komine R (1999) Effect of W on recovery of lath structure during creep of high chromium martensitic steels. Mater Sci Eng A 267:19–25. https://doi.org/10.1016/S0921-5093(99)00066-0

[61] Polcik P, Sailer T, Blum W, Straub S, Buršík J, Orlová A (1999) On the microstructural development of the tempered martensitic Cr-steel P 91 during long-term creep—a comparison of data. Mater Sci Eng A 260:252–259. https://doi.org/10.1016/S0921-5093(98)00887-9

[62] Kostka A, Tak K, Hellmig R, Estrin Y, Eggeler G (2007) On the contribution of carbides and micrograin boundaries to the creep strength of tempered martensite ferritic steels. Acta Mater 55:539–550. https://doi.org/10.1016/j.actamat.2006.08.046

[63] Wang H, Yan W, van Zwaag S, Shi Q, Wang W, Yang K, Shan Y (2017) On the 650 °C thermostability of 9–12Cr heat resistant steels containing different precipitates. Acta Mater 134:143–154. https://doi.org/10.1016/j.actamat.2017.05.069

[64] Mishnev R, Dudova N, Kaibyshev R (2018) On the origin of the superior long-term creep resistance of a 10% Cr steel. Mater Sci Eng A 713:161–173. https://doi.org/10.1016/j.msea.2017.12.066

[65] Eggeler G (1989) The effect of long-term creep on particle coarsening in tempered martensite ferritic steels. Acta Metall 37:3225–3234. https://doi.org/10.1016/0001-6160(89)90194-6

[66] Nakajima T, Spigarelli S, Evangelista E, Endo T (2003) Strain enhanced growth of precipitates during creep of T91. Mater Trans JIM 44:1802–1808. https://doi.org/10.2320/matertrans.44.1802

[67] Magnusson H, Sandström R (2007) Creep strain modeling of 9 to 12 Pct Cr steels based on microstructure evolution. Metall Mater Trans A 38:2033–2039. https://doi.org/10.1007/s11661-007-9256-9

[68] Fedoseeva A, Dudova N, Kaibyshev R (2017) Creep behavior and microstructure of a 9Cr–3Co–3W martensitic steel. J Mater Sci 52:2974–2988. https://doi.org/10.1007/s10853-016-0595-z

[69] Isik MI, Kostka A, Yardley VA, Pradeep KG, Duarte MJ, Choi PP, Raabe D, Eggeler G (2015) The nucleation of Mo-rich Laves phase particles adjacent to M23C6 micrograin boundary carbides in 12% Cr tempered martensite ferritic steels. Acta Mater 90:94–104. https://doi.org/10.1016/j.actamat.2015.01.027

[70] Cui H, Sun F, Chen K, Zhang L, Wan R, Shan A, Wu J (2010) Precipitation behavior of Laves phase in 10%Cr steel X12CrMoWVNbN10-1-1 during short-term creep exposure. Mater Sci Eng A 527:7505–7509. https://doi.org/10.1016/j.msea.2010.08.013

[71] Hald J (1996) Metallurgy and creep properties of new 9–12%Cr steels. Steel Res 67:369–374. https://doi.org/10.1002/srin.199605503

[72] Wang X, Xu Q, Yu S-m, Hu L, Liu H, Ren Y-y (2015) Laves-phase evolution during aging in 9Cr-1.8W-0.5Mo-

VNb steel for USC power plants. Mater Chem Phys 163:219–228. https://doi.org/10.1016/j.matchemphys.2015.07.032

[73] Abe F (2005) Effect of fine precipitation and subsequent coarsening of Fe2W laves phase on the creep deformation behavior of tempered martensitic 9Cr-W steels. Metall Mater Trans A 36:332. https://doi.org/10.1007/s11661-005-0305-y